Journal of Power Sources 182 (2008) 83–90

Contents lists available at ScienceDirect

Journal of Power Sources

journal homepage: www.elsevier.com/locate/jpowsour

Evaluation of the stability and durability of Pt and Pt–Co/C catalysts for polymer electrolyte membrane fuel cells

Sabrina C. Zignani[a], Ermete Antolini[a,b], Ernesto R. Gonzalez[a,*]

[a] Instituto de Química de São Carlos, USP, C.P. 780, São Carlos 13560-970, SP, Brazil
[b] Scuola di Scienza dei Materiali, Via 25 aprile 22, 16016 Cogoleto, Genova, Italy

ARTICLE INFO

Article history:
Received 1 February 2008
Received in revised form 12 March 2008
Accepted 16 March 2008
Available online 30 March 2008

Keywords:
Oxygen reduction
Pt–Co/C electrocatalysts
PEM fuel cell
Dissolution
Stability

ABSTRACT

Carbon supported Pt and Pt–Co nanoparticles were prepared by reduction of the metal precursors with $NaBH_4$. The activity for the oxygen reduction reaction (ORR) of the as-prepared Co-containing catalyst was higher than that of pure Pt. 30 h of constant potential operation at 0.8 V, repetitive potential cycling in the range 0.5–1.0 V and thermal treatments were carried out to evaluate their electrochemical stability. Loss of non-alloyed and, to a less extent, alloyed cobalt was observed after the durability tests with the Pt–Co/C catalyst. The loss in ORR activity following durability tests was higher in Pt–Co/C than in Pt/C, i.e. pure Pt showed higher electrochemical stability than the binary catalyst. The lower stability of the Pt–Co catalyst during repetitive potential cycling was not ascribed to Co loss, but to the dissolution–re-deposition of Pt, forming a surface layer of non-alloyed pure Pt. The lower activity of the Pt–Co catalyst than Pt following the thermal treatment, instead, was due to the presence of non-alloyed Co and its oxides on the catalyst surface, hindering the molecular oxygen to reach the Pt sites.

1. Introduction

Platinum is known to present the best catalytic activity for the oxygen reduction reaction (ORR) among all pure metals and when supported on a conductive carbon serves as state of the art electrocatalyst in low temperature fuel cell air cathodes [1]. However, due to kinetic limitations of the oxygen reduction reaction the cathodic overpotential losses amount to 0.3–0.4 V under typical polymer electrolyte fuel cell (PEMFC) operating conditions [1]. In addition, Pt is expensive and the world's supply is limited. Therefore, the development of more active and less expensive oxygen reduction electrocatalysts than pure Pt has been the subject of extensive research for a number of decades and has favored the use of suitable Pt-alloys. Among these, recent studies reported that Pt–Co alloys show enhanced catalytic activity compared to pure Pt for oxygen reduction [2–15].

Catalyst durability is an additional factor for consideration, limiting the commercialization of PEMFCs. Metal particle sintering, metal dissolution and corrosion of the carbon support contribute to the degradation of the cathode catalyst. The results of different tests on the stability of Pt–M alloy catalysts under fuel cell conditions and the consequences on the electrocatalytic activity and cell performance have been reviewed by Antolini et al. [15]. Various papers focused on the stability of Pt–Co catalysts in a fuel cell environment. Beard and Ross [16] and Travitsky et al. [17] investigated the stability of Pt–Co catalysts (Co loss, changes in the lattice parameter and in the surface area) but did not investigate its effect on the ORR activity. Watanabe et al. [18] compared the ORR activity of ordered and disordered Pt–Co alloys after durability tests (the disordered alloy was found to be more stable than the ordered alloy) but no comparison was made with pure Pt. Yu et al. [19] investigated the durability of Pt/C and Pt–Co/C cathode catalysts in a dynamic fuel cell environment with continuous water fluxing on the cathode. A potential cycling test between 0.87 and 1.2 V vs. RHE was applied to the system to illustrate how cobalt or platinum dissolution affect the cell performance. They found that cobalt dissolution neither detrimentally reduces the cell voltage nor dramatically affects the membrane conductance. Colón-Mercado and Popov [20] investigated the corrosion and surface area changes of platinum based catalysts supported on carbon and found a strong correlation between the amount of the alloying metal dissolved and the ORR activity of the Pt-alloy catalysts.

In this work, carbon supported Pt and Pt–Co catalysts were prepared by reduction of the corresponding metal precursors with $NaBH_4$ at room temperature, to avoid the sintering of metal particles that takes place when the synthesis of the catalyst is carried out at high temperatures [21]. Then, the durability of Pt and Pt–Co electrocatalysts was investigated by correlating the changes of electrocatalyst characteristics (Co content, lattice parameter, particle size) and the loss of ORR activity observed after various types

* Corresponding author. Tel.: +55 16 33739899; fax: +55 16 33739952.
E-mail address: ernesto@iqsc.usp.br (E.R. Gonzalez).

0378-7753/$ – see front matter © 2008 Elsevier B.V. All rights reserved.
doi:10.1016/j.jpowsour.2008.03.061

of testing. Different types of durability tests were carried out: (i) 30 h of constant potential (CP) operation at 0.8 V, (ii) repetitive potential cycling (RPC) at 20 mV s^{-1} between 0.5 and 1 V (cycle number = 1000), (iii) thermal treatment (TT) at 550 °C for 1 h in a H_2 atmosphere, and (iv) TT + RPC.

2. Experimental

Carbon supported Pt and Pt–Co (nominal Pt:Co atomic ratio 75:25) electrocatalysts were prepared by a low temperature method, using sodium borohydride as the reducing agent. High surface area carbon (Vulcan XC-72R, Cabot, 240 m^2 g^{-1}) was impregnated with a solution of chloroplatinic acid ($H_2PtCl_6{\cdot}6H_2O$, Johnson Matthey) and, in the case of Pt–Co, cobalt hydroxide ($Co(OH)_2{\cdot}6H_2O$, Aldrich) solution as well. The metals were then reduced at room temperature with a sodium borohydride solution, which was slowly added to the precursors dispersion under sonication. The resulting material was 20 wt.% metal on carbon.

The atomic ratio of the Pt–Co/C catalysts was determined by the EDX technique coupled to a scanning electron microscopy LEO Mod. 440 with a silicon detector with Be window and applying 20 keV.

X-ray diffractograms of the electrocatalysts were obtained in a universal diffractometer Carl Zeiss-Jena, URD-6, operating with Cu Kα radiation (λ = 0.15406 nm) generated at 40 kV and 20 mA. Scans were done at 3° min^{-1} for 2θ values between 20° and 100°. It has to be remarked that the diffractograms of the as-prepared and thermally treated catalysts were obtained with the catalyst powder, whereas the XRD analysis on the catalysts submitted to RPC were carried out on the electrode. An average value of the lattice parameters was obtained from the Pt (1 1 1), (2 0 0), (2 2 0) and (3 1 1) peaks. The crystallite sizes were obtained from the Pt (2 2 0) reflection using Scherrer's equation. Previous studies on Pt–Co catalysts prepared in this laboratory [11–13] showed that crystallite and particle sizes are very similar, which allows an estimation of the roughness factor.

The electrodes used in this work were two layer gas diffusion electrodes (GDE). A diffusion layer was made by mixing carbon powder (Vulcan XC-72R) and 30 wt.% polytetrafluoroethylene (PTFE) and the mixture applied over a carbon cloth (PWB-3, Stackpole). On top of this layer, the electrocatalyst was applied in the form of a homogeneous dispersion of Pt–Co/C, or Pt/C, Nafion® solution (5 wt.%, Aldrich) and isopropanol (Merck). All electrodes were made to contain 0.4 mg cm^{-2} of metal. Electrochemical experiments were performed with these electrodes, containing Pt–Co/C or Pt/C as catalysts, in a three-compartment PTFE half-cell with a volume of approximately 70 mL. The working electrode compartment contained suitable inlets and outlets to feed gaseous reagents to the GDE. A reversible hydrogen electrode was used as reference and a platinum foil electrode as auxiliary. The electrochemical experiments were done at room temperature with a 1285A Solartron Potentiostat connected to a personal computer and using the software CorrWare for Windows (Scribner).

Linear sweep curves (LSV) in the range 0.1–1.0 V and cyclic voltammograms (CV) were recorded in a 0.5 M H_2SO_4 solution, at a sweep rate of 20 mV s^{-1}.

Two types of constant potential (CP) experiments were carried out at 0.8 V also in a 0.5 M H_2SO_4 solution. Normal chronoamperometry (CA) was performed for 3600 s to test the activity of the catalysts under quasi-steady-state conditions. Extended experiments for 30 h were performed separately to evaluate the durability of the catalysts. In this case, every 5 h of testing the H_2SO_4 solution in the cell was changed by a fresh one and submitted to atomic absorption analysis to determine Pt and Co eventually dissolved. Atomic absorption (AA) determinations were carried out using an Atomic Absorption Spectrophotometer HITACHI Z-8100.

The sequence of experiments in this work was as follows. The as-prepared catalysts were submitted to LSV and CA experiments in an oxygen saturated solution to evaluate the activity for the ORR. Next, under an inert argon atmosphere, they were submitted to a durability experiment involving either 30 h of constant potential (0.8 V vs. RHE) operation or repetitive potential cycling (1000 cycles) between 0.5 and 1.0 V vs. RHE at 20 mV s^{-1}. After the durability test, the solution was again saturated with oxygen and LSV and CA experiments were performed again.

3. Results and discussion

3.1. As-prepared catalysts

Three samples of the Pt–Co electrocatalyst were submitted to EDX analysis and the results were similar, indicating good homogeneity. Also, the EDX atomic composition in various parts of the nanoparticle powders was about 77:23, which is very close to the nominal value.

Fig. 1 shows the X-ray diffraction patterns of the Pt/C and Pt–Co/C electrocatalysts, where the peak at 20–25° is attributed to the (0 0 2) plane of the hexagonal structure of the Vulcan XC-72R carbon. As indicated in Fig. 1, both XRD patterns show the five main characteristic peaks of the face-centered cubic (fcc) crystalline Pt, namely, the planes (1 1 1), (2 0 0), (2 2 0), (3 1 1), and (2 2 2). In the Pt–Co/C electrocatalyst the peaks are slightly shifted to higher angles with respect to those in the Pt/C electrocatalyst, indicating a contraction of the lattice and alloy formation. No superlattice reflections were present in the XRD pattern of Pt–Co, which indicates the formation of only a disordered solid solution. Also, no peaks for pure Co or its oxides was found, but their presence cannot be discarded because they may be present in a small amount or even in an amorphous form. The lattice parameters of the electrocatalysts are reported in Table 1 and show a smaller value for Pt–Co/C than for Pt/C, reflecting the introduction of Co into the alloyed state. Assuming that Vegard's law applies to Pt–Co solid solutions, the Co atomic fraction in the Pt–Co alloy (x) was evaluated by the linear relationship:

$$x = \left[\frac{a - a_o}{a_s - a_o}\right] x_s \quad (1)$$

where a_o and a_s are the lattice parameters of Pt (0.3925 nm) and Pt_3Co (0.3831 nm [16]), and x_s is the Co atomic fraction (0.25) in the Pt_3Co catalyst. To a rough approximation, assuming that all Pt is alloyed with Co, the degree of alloy, i.e. the ratio of alloyed Co

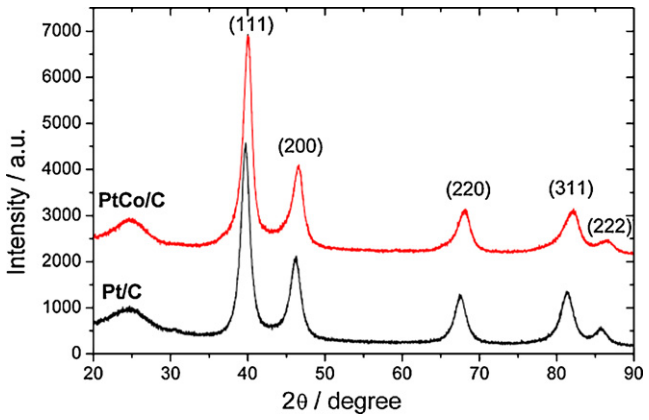

Fig. 1. XRD diffractograms of as-prepared Pt/C and Pt–Co/C electrocatalysts.

Table 1
EDX composition, lattice parameter, Co atomic fraction in the alloy (x), degree of alloying, crystallite size, roughness factor (RF) and steady-state current density at 0.8 V from chronoamperometry, expressed both on the basis of geometric area (i) and specific area (i_{Norm}), of as-prepared Pt/C and Pt–Co/C catalysts

Catalyst	EDX	Lattice parameter (nm)	x	Degree of alloy	Crystallite size (nm)	RF	i (mA cm^{-2})	i_{Norm} (μA cm^{-2})
Pt–Co/C	77:23	0.38967	0.076	0.28	5.1	20.6	15.3	743
Pt/C	–	0.39252	0.00		5.5	20.3	10.7	527

(Co_{al}) to total Co in the catalyst (Co_{tot}) is given by:

$$\frac{Co_{al}}{Co_{tot}} = \frac{xPt_{EDX}}{(1-x)Co_{EDX}} \quad (2)$$

where Pt_{EDX} and Co_{EDX} are the actual EDX atomic compositions of Pt and Co, respectively. The values of x and Co_{al}/Co_{tot} are given in Table 1. The average crystallite sizes of the Pt and Pt–Co catalysts, estimated using Scherrer's equation, were 5.5 and 5.1 nm, respectively.

The electrochemical activity for oxygen reduction of the as-prepared Pt/C and Pt–Co/C catalysts was investigated by linear sweep voltammetry (LSV) experiments in H_2SO_4 solution at room temperature. The experimental results are shown in Fig. 2a, with the current density expressed in terms of the geometric surface area. The onset potential for the ORR was about the same for Pt–Co/C and Pt/C, about 850 mV, but the slope of the current density–potential plot (dj/dE), for Pt–Co/C was slightly larger than for Pt/C meaning that the activity for the ORR of the Pt–Co/C catalyst

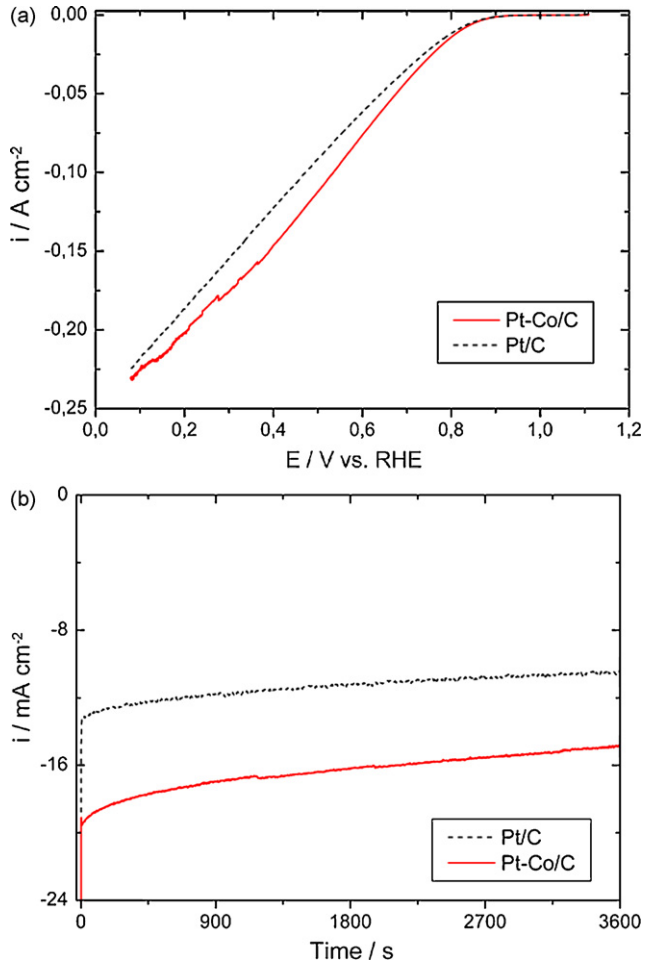

Fig. 2. (a) Oxygen reduction at room temperature in 0.5 M H_2SO_4 on as-prepared Pt–Co/C and Pt/C electrocatalysts. Current densities normalized with respect to the geometric surface area. (b) Chronoamperometry test for oxygen reduction at room temperature on Pt/C and Pt–Co/C electrocatalysts.

Table 2
EDX composition, Co and Pt loss by AA, Pt:Co composition from AA results and steady-state current density from CA of as-prepared Pt/C and Pt–Co/C catalysts after 30 h of operation at 0.8 V

Catalyst	EDX	Co loss by AA (%)	Pt loss by AA (%)	Pt:Co from AA	i (mA cm^{-2})
Pt–Co/C	94:6	79	7	93.7:6.3	12.9
Pt/C	–	–	Undetected		10.1

is higher. In terms of overpotential, at a current density of 0.1 A cm^{-2} the overpotential on Pt–Co/C was about 60 mV less compared to that on Pt/C.

The results of the chronoamperometry (CA) tests for oxygen reduction at 0.8 V for 3600 s are shown in Fig. 2b. After the initial surge due to the charging current, the currents for oxygen reduction decrease rapidly at first and then became relatively stable. Consistent with the LSV results, the steady-state current density, expressed in terms of both geometric area and specific surface area (see Table 1), on the as-prepared Pt–Co/C catalyst is significantly larger than that on Pt/C.

The improvement in ORR activity of Pt-alloys has been ascribed to different structural changes caused by alloying, as electronic (Pt d-band vacancy [22]) and geometric (Pt–Pt bond distance [23]) modifications. Recently, Toda et al. [24] studied the ORR activity of bulk Pt alloys with Ni, Co and Fe at room temperature, and observed larger kinetic current densities than that on pure Pt. By XPS experiments they found that Ni, Co or Fe disappeared from all the alloy surface layers and the active surfaces were covered by a Pt skin of a few monolayers, with a different electronic structure than that of the bulk alloys. Also, Stamenkovic et al. [25,26] studied the intrinsic catalytic activity of Pt_3Ni and Pt_3Co bulk alloy catalysts for the ORR and, in agreement with Toda et al. [24], observed that the "Pt-skin" structure is more active than both pure Pt and Pt_3Co alloy surfaces. They suggested that the catalytic improvement is due to electronically modified Pt atoms on the top of the Co-enriched layer.

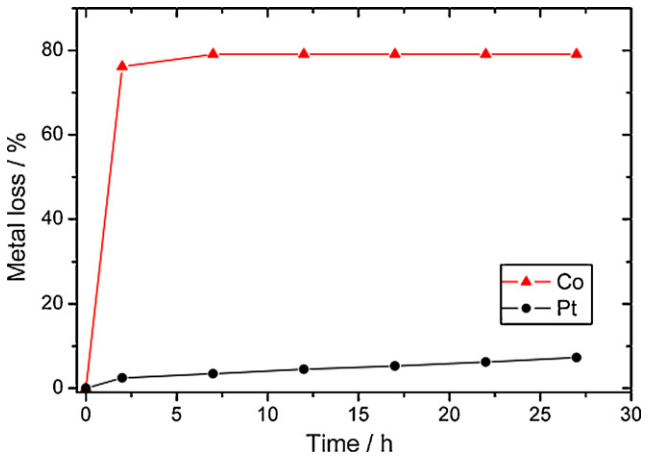

Fig. 3. Pt and Co loss from the Pt–Co/C catalyst determined by atomic absorption in the solution vs. testing time.

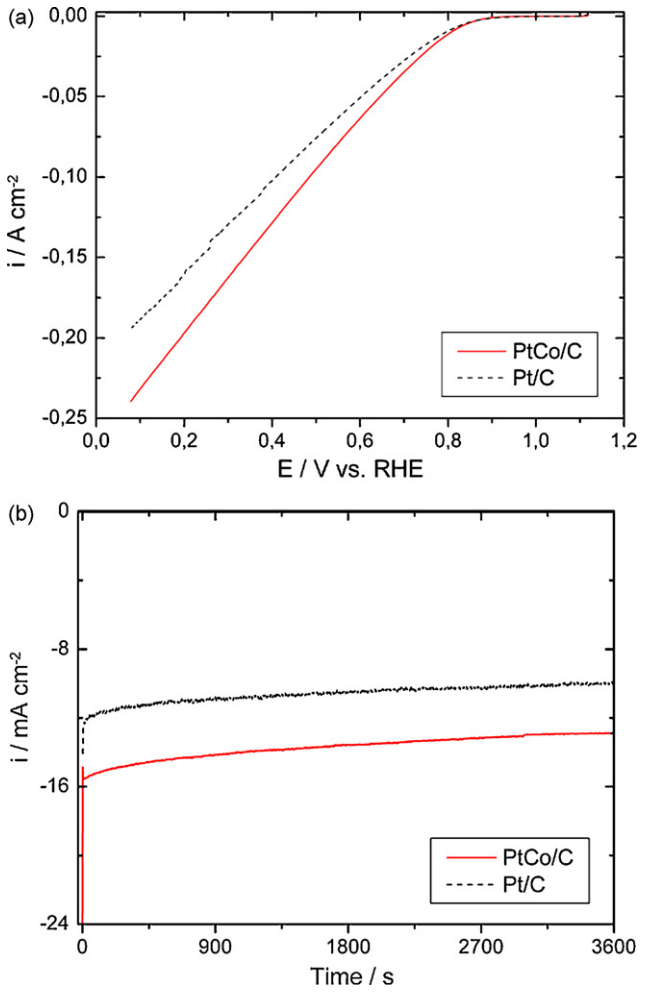

Fig. 4. (a) Oxygen reduction at room temperature in 0.5 M H_2SO_4 on Pt–Co/C and Pt/C electrocatalysts following 30 h CP at 0.8 V. Current densities normalized with respect to the geometric surface area. (b) Chronoamperometry test for oxygen reduction at room temperature on Pt/C and Pt–Co/C electrocatalysts.

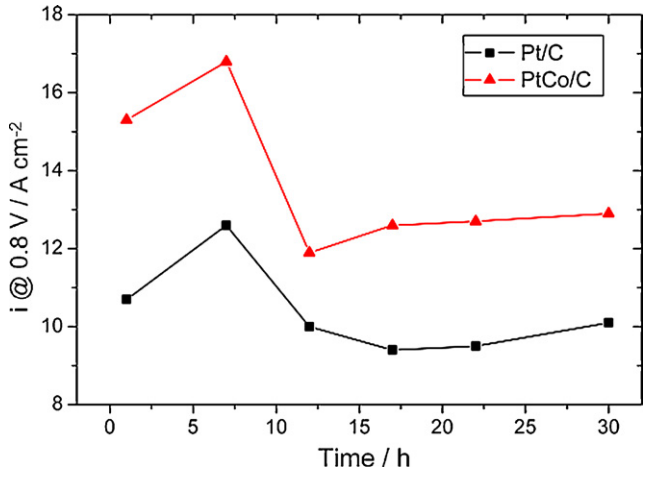

Fig. 5. Dependence of the steady-state current density of oxygen reduction at 0.8 V on testing time.

3.2. Extended constant potential experiments

Following 30 h of CP at 0.8 V, the average EDX Pt:Co composition of the Pt–Co/C catalyst was 94:6, as reported in Table 2, indicating that the Co content in the Pt–Co/C catalyst decreased significantly. The amount of Co lost to the solution was obtained from atomic absorption analysis, and led to the conclusion that Co loss occurs in the first 7 h of the operation test, as shown in Fig. 3. Contrary to the case of Pt/C, Pt loss from Pt–Co/C was also observed all along the operation test (see Fig. 3) indicating that Pt dissolves from the Pt–Co alloy, not from Pt oxides eventually present. Likely, Co also dissolves from the Pt–Co alloy but the Co fraction in the alloy ($x = 0.076$) is so small that the amount dissolved from the alloy cannot be detected. From the fractions of Co loss (y_{CoL}) and Pt loss (y_{PtL}) the Co atomic fraction remaining in the catalyst after the CP test (x_{CoR}) was calculated using the following relationship:

$$x_{CoR} = \frac{(1 - y_{CoL})Co_{EDX}}{(1 - y_{CoL})Co_{EDX} + (1 - y_{PtL})Pt_{EDX}} \quad (3)$$

where Co_{EDX} and Pt_{EDX} are the EDX Co and Pt atomic fractions before the CA test, respectively. The obtained value was 0.063, in close agreement with the value from EDX after testing (0.06). In agreement with previous reported results [15], Co loss was considered as coming mainly from non-alloyed Co but, being the amount of Co remaining lower than the amount of Co alloyed, it must be concluded that part of the Co alloyed also dissolved during the 30 h CP test.

Fig. 4 shows the LSV (Fig. 4a) and CA (Fig. 4b) plots in the presence of oxygen for Pt/C and Pt–Co/C after 30 h of constant potential test, respectively. A comparison of these curves with those shown in Fig. 2a and b, shows very little changes in the ORR activity, being the decrease in steady-state current densities at 0.8 V 5% for Pt/C and 16% for Pt–Co/C.

Fig. 5 shows the dependence of the steady-state current density for oxygen reduction at 0.8 V on testing time. For both catalysts an increase of the current density took place in the first 7 h, due to Co loss in the Pt–Co/C catalyst and to the cleaning of impurities in Pt/C. From 7 to 12 h a decrease was observed, due to a rearrangement of the metal particle packing with reduction of the surface area. Finally, for times longer than 12 h a slight increase in the current density was observed for the two catalysts.

3.3. Repetitive potential cycling (RPC)

As reported by Borup et al. [27], the ageing test by repetitive potential cycling is more severe than that under steady-state conditions. EDX analysis on Pt–Co/C following RPC showed a less homogeneous distribution of Co than that in the as-prepared material. The average Pt:Co composition was 91:9, as reported in Table 3. By AA analysis Pt loss was observed from both catalysts (Table 3) and Co loss from Pt–Co/C. The Pt:Co composition calculated by Eq. (3) using the amounts of Co and Pt lost to

Table 3
EDX composition, Co and Pt loss by AA, Pt:Co composition from AA results, lattice parameter, Co atomic fraction in the alloy (x) and crystallite size of as-prepared Pt/C and Pt–Co/C catalysts after repetitive potential cycling

Catalyst	EDX	Co loss by AA (%)	Pt loss by AA (%)	Pt:Co from AA	Lattice parameter (nm)	x	Crystallite size (nm)
Pt–Co/C 77:23	91:9	64.5	6.9	90:10	0.39015	0.063	6.1
Pt/C	–	–	6.7		0.39224		6.6

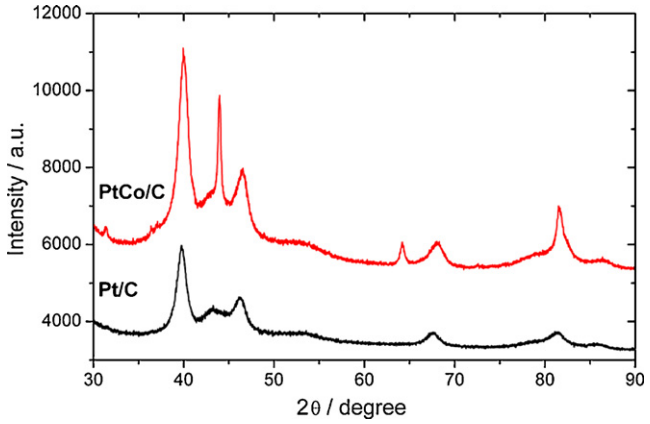

Fig. 6. XRD diffractograms of as-prepared Pt/C and Pt–Co/C electrocatalysts following repetitive potential cycling.

the solution was in close agreement with the EDX composition.

Fig. 6 shows the XRD patterns of Pt–Co/C and Pt/C after repetitive potential cycling obtained with the entire electrode, i.e. in the presence of the different materials forming the electrode other than the catalyst. For Pt–Co/C the presence of three unknown peaks at 2θ values about 44°, 64° and 81° (the last overlapped to the Pt (3 1 1) peak) was observed. These three reflections were also present in both the Pt–Co/C and Pt/C catalysts thermally treated and submitted to potential cycling, as shown below. The lattice parameter of the Pt–Co catalyst after RPC was higher than that of the as-prepared catalyst, which was ascribed to a lower Co content in the alloy, in agreement with the result observed after 30 h CP, i.e. Co dissolution from the alloy. As shown in Table 3, the amount of Co alloyed was lower than the amount of Co remaining in the catalyst, meaning that non-alloyed Co is still present in the catalyst after cycling.

Following RPC, both catalysts presented a 20% increase of the crystallite size with respect to the as-prepared catalysts (see Table 3), which agrees with the reported growth of metal particles of supported catalysts submitted to RPC [28–35]. Also, repetitive potential cycling dissolves Pt (and Co) atoms [33,34] which results in a roughening of the surface [35]. Based on results obtained by chemical, XRD and TEM with EDS analyses, Watanabe et al. [18] suggested that the corrosion mechanism of Pt–Co alloy catalysts involves the dissolution of Co and Pt from small-size alloy particles and the re-deposition of Pt on the surface of larger particles. Indeed, a surface-enrichment with Pt has been observed after potential cycling [34], which in binary alloys is associated to the dissolution of the less noble component. The thick Pt layer formed by dissolution–re-deposition of Pt is different from the dealloyed thin layer, prepared by sputtering, described by Toda et al. [24]. In this case, the growth of the Pt skin may be limited to few monolayers and hence its electronic properties are appreciably modified by the underlying bulk alloy. Indeed, according to Toda et al. [24], the effect must be reduced for increasing thicknesses of the Pt skin, resulting in a lower enhancement effect by alloying.

Fig. 7 shows the LSV (Fig. 7a) and CA (Fig. 7b) plots for Pt/C and Pt–Co/C after RPC, respectively, in the presence of oxygen. After potential cycling both catalysts present smaller current densities, due to the increase in particle size, and about the same ORR activity, while the overpotentials at high potentials are quite similar (Fig. 7a). This indicates that the formation of a Pt layer on the surface of the Pt–Co catalyst cancelled the positive effect of Co alloying and, as a result, the steady-state current density at 0.8 V in CA experiments decreases much more for the binary catalyst than for pure Pt (18% for Pt/C and 50% for Pt–Co/C).

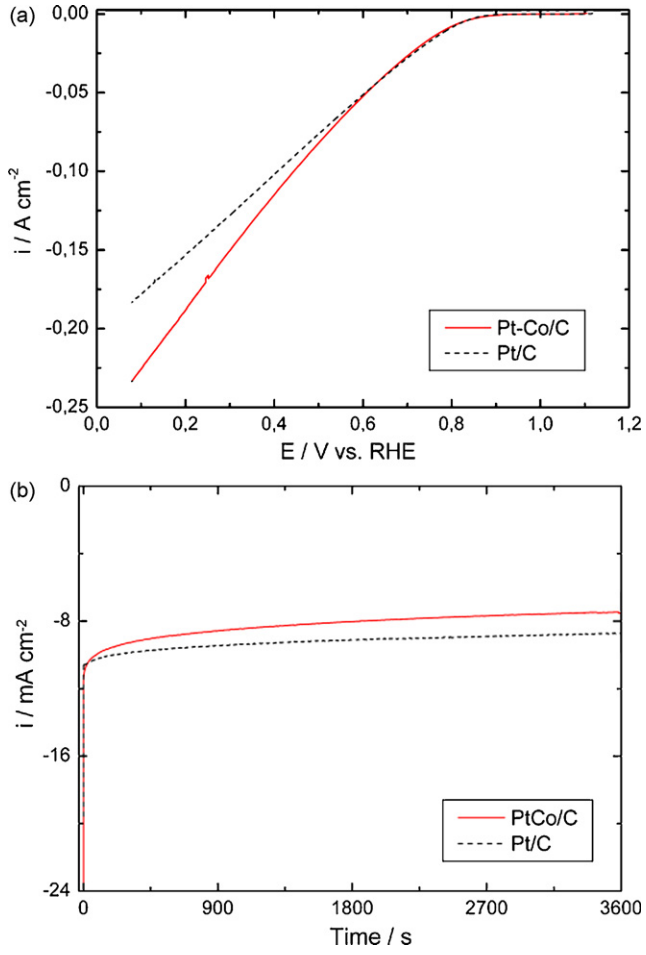

Fig. 7. (a) Oxygen reduction at room temperature in 0.5 M H_2SO_4 on as-prepared Pt–Co/C and Pt/C electrocatalysts after RPC. Current densities normalized with respect to the geometric surface area. (b) Chronoamperometry test for oxygen reduction at room temperature on Pt/C and Pt–Co/C electrocatalysts.

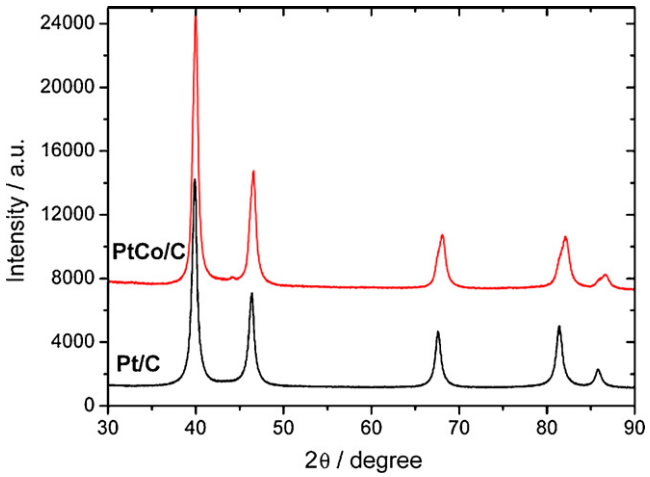

Fig. 8. XRD diffractograms of thermally treated Pt/C and Pt–Co/C electrocatalysts.

3.4. Thermal treatment (TT)

The XRD patterns of Pt/C and Pt–Co/C following thermal treatment at 550 °C in a hydrogen atmosphere for 1 h are shown in Fig. 8. The lattice parameter of Pt–Co/C was about the same as that of the as-prepared catalyst, i.e. the amount of Co alloyed did not increase

Table 4
Lattice parameter, Co atomic fraction in the alloy (x), degree of alloy and crystallite size of thermally treated Pt/C and Pt–Co/C catalysts

Catalyst	attice parameter (nm)	x	Degree of alloy	Crystallite size (nm)
Pt–Co/C 77:23	0.38978	0.073	0.26	9.3
Pt/C	0.39171			13

with the thermal treatment, showing that a temperature of 550 °C is not high enough to promote alloy formation [21]. The sharp Pt and Pt–Co reflections indicate the formation of larger crystallites, due to sintering and coalescence, the increase being 82% for Pt–Co and of 138% for Pt with respect to the as-prepared catalysts, as shown in Table 4. This shows that Pt–Co particles grow less than Pt particles as a consequence of the thermal treatment, in agreement with reports in the literature for Pt–Co alloys [11,20], and can be explained by the increased sintering resistance due to the presence of the alloying elements, i.e., the anchor effects of the alloying element on the carbon substrates.

The LSV and CA plots in the presence of oxygen for Pt/C and Pt–Co/C after the thermal treatment are presented in Fig. 9a and b, respectively, which show a lower ORR activity with respect to the as-prepared catalysts due to the increase in particle size. Notwithstanding a larger crystallite size than the Co containing catalyst, pure Pt shows a considerably higher ORR activity with an overpotential at a current density of 0.1 A cm^{-2} about 150 mV lower compared to that on Pt–Co/C. Consistent with the LSV results, the steady-state current density at 0.8 V from CA on the as-prepared Pt–Co/C catalyst was significantly lower than that on Pt/C. Investigations of surface-enrichment phenomena [36–38] carried out on Pt–Rh showed that, whereas potential cycling conditions lead to preferential dissolution of rhodium and, as a consequence, to surface enrichment with Pt, heat treatment gives rise to surface enrichment with rhodium. Analogously, it can be expected that surface enrichment with Co occurs on Pt–Co following the thermal treatment. On this basis, the lower ORR activity of Pt–Co could be ascribed to the negative effect of surface enrichment with non-alloyed Co and its oxides due to the thermal treatment, hindering the molecular oxygen to reach Pt active sites.

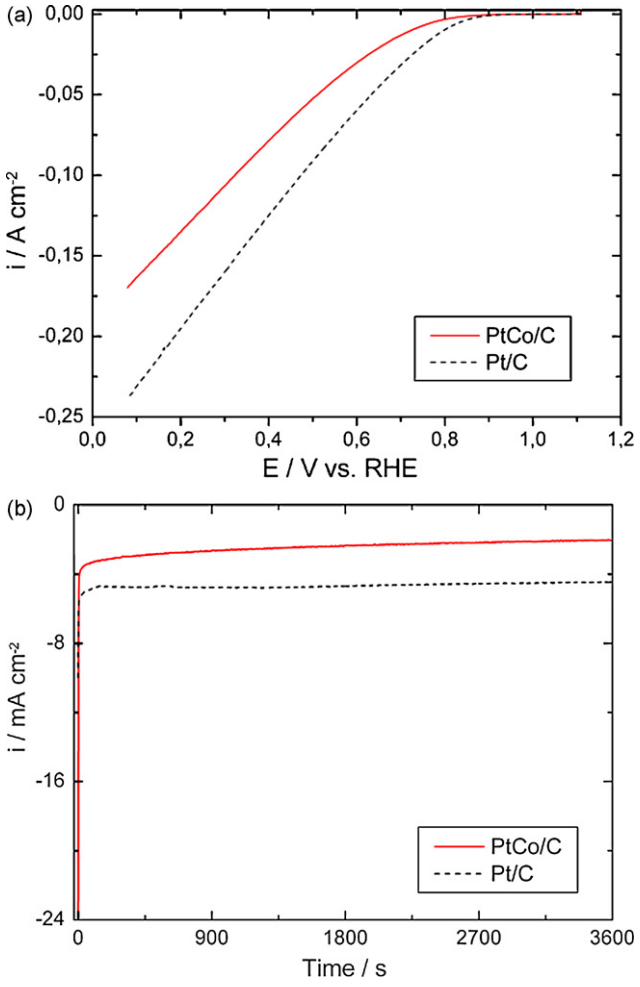

Fig. 9. (a) Oxygen reduction at room temperature in 0.5 M H_2SO_4 on thermally treated Pt–Co/C and Pt/C electrocatalysts. Current densities normalized with respect to the geometric surface area. (b) Chronoamperometry test for oxygen reduction at room temperature on Pt/C and Pt–Co/C electrocatalysts.

3.5. Thermal treatment and repetitive potential cycling

The average Pt:Co composition of thermally treated Pt–Co/C following RPC was 96:4, as reported in Table 5. Atomic adsorption analysis indicated a loss of Pt in both catalysts, and also of Co in the Pt–Co sample (Table 5). The composition determined from AA results was higher than the EDX composition: as the measurements were made not on the powder (as in the case of the sample not submitted to potential cycling) but on the electrode, the EDX analysis could be more influenced by the surface composition (poorer in Co). Fig. 10 shows the XRD patterns of thermally treated Pt/C and Pt–Co/C following RPC. Curiously, the lattice parameter of Pt (Table 5) was higher than the values commonly observed (0.3915–0.3925 nm), and at this stage it can only be suggested that it is due to the formation of a Pt alloy with some metal present as an impurity. The Co content in the alloy was quite similar to that in the thermally treated Pt–Co/C before RPC (the slight difference in the lattice parameter may be due to different particle sizes). Probably, Co loss on potential cycling occurs from non-alloyed Co at the surface of the particles but, due to the large crystallite size, XRD measurements reveal the bulk composition, which is not affected by cycling. As shown in Table 5, a slight increase in particle size occurred during RPC, 5% for Pt–Co, and 15% for Pt and, as in the case of the as-prepared catalysts, dissolution–re-deposition of Pt is expected to take place during RPC on thermally treated samples.

Fig. 11 shows the LSV (Fig. 11a) and CA (Fig. 11b) plots for oxygen reduction on thermally treated Pt/C and Pt–Co/C, respectively, after RPC. Fig. 11a shows that the overpotential on thermally treated Pt–Co/C at a current density of 0.1 A cm^{-2} is not as large with respect to that on Pt/C as before RPC (85 mV vs. 150 mV) and that the steady-state current density at 0.8 V (Fig. 11b) was almost the same as that on Pt. This is because during repetitive potential cycling non-alloyed Co and its oxides dissolve and, as a consequence, the ORR activity is larger than that of thermally treated Pt–Co/C before

Table 5
EDX composition, Co and Pt loss by AA, Pt:Co composition from AA, lattice parameter and crystallite size of thermally treated Pt/C and Pt–Co/C catalysts after repetitive potential cycling

Catalyst	EDX composition	Co loss by AA (%)	Pt loss by AA (%)	Pt:Co by AA	Lattice parameter (nm)	Crystallite size (nm)
Pt–Co	96:4	59.1	8.3	88:12	0.38953	9.8
Pt					0.39430	15.1

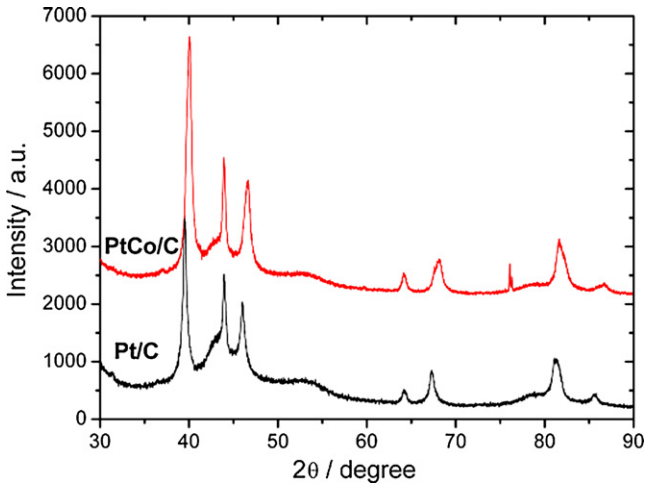

Fig. 10. XRD diffractograms of thermally treated Pt/C and Pt–Co/C electrocatalysts following repetitive potential cycling.

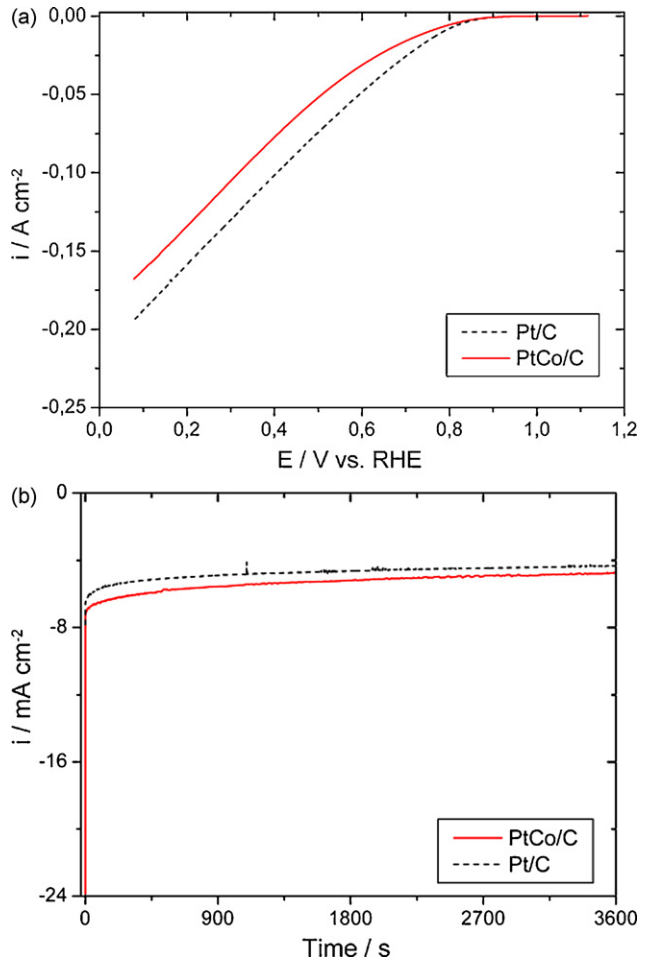

Fig. 11. (a) Oxygen reduction at room temperature in 0.5 M H_2SO_4 on thermally treated Pt–Co/C and Pt/C electrocatalysts after RPC. Current densities normalized with respect to the geometric surface area. (b) Chronoamperometry test for oxygen reduction at room temperature on Pt/C and Pt–Co/C electrocatalysts.

the cycling test. Also in this case, Pt surface enrichment occurs by repetitive potential cycling.

Fig. 12 shows the dependence of the steady-state current density at 0.8 V of all Pt/C catalysts (as-prepared, TT and submitted to RPC) and of Pt–Co/C following RPC (catalyst surface similar to pure Pt) on crystallite size and shows that the ORR activity of these catalysts seems to depend only on crystallite size. The histogram of the steady-state current density for oxygen reduction from CA of Pt–Co/C and Pt/C catalysts before and after stability tests is shown in Fig. 13. The difference in ORR activity (steady-state current density at 0.8 V from CA) before and after potential cycling for as-prepared and thermally treated Pt/C and Pt–Co/C is shown in Fig. 14 and shows a substantial stability of Pt/C with regards to its electrochemical activity, which decreases slightly due to the increase in the crystallite size. On the other hand, a relatively large effect of RPC on the ORR activity of Pt–Co/C can be observed (Fig. 14). In

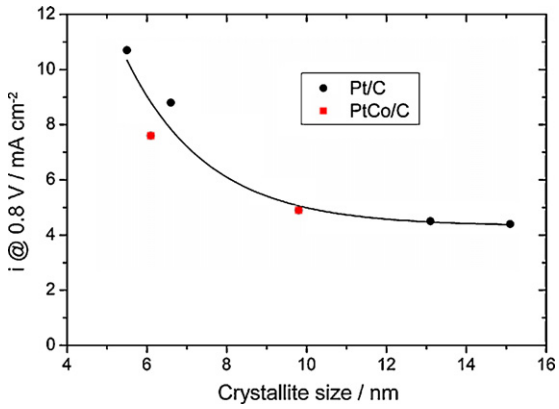

Fig. 12. Dependence of the steady-state current density at 0.8 V for all Pt/C catalysts (as-prepared, TT and submitted to RPC) and for Pt–Co following RPC on crystallite size.

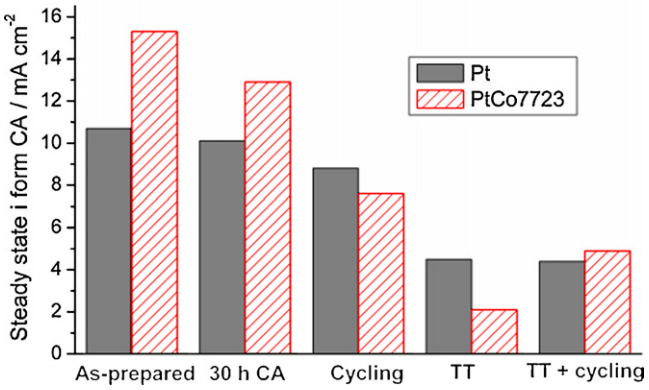

Fig. 13. Histogram of the steady-state current densities of oxygen reduction from CA of Pt–Co/C and Pt/C catalysts before and after stability tests.

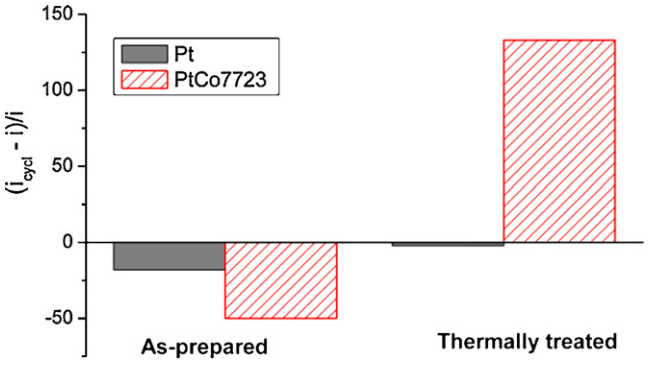

Fig. 14. Histogram of the difference in the steady-state current densities at 0.8 V before and after potential cycling for as-prepared and thermally treated Pt/C and Pt–Co/C.

the case of the as-prepared catalyst this is due to Pt re-deposition, which eliminates the positive effect of Co alloying on the oxygen reduction, whereas in the case of the thermally treated sample it is ascribed to both re-deposition of Pt and dissolution of non-alloyed Co, which eliminate the negative effect of Co surface enrichment on the activity for the ORR.

4. Conclusions

As-prepared Pt–Co/C catalysts presented higher ORR activity than Pt/C.

The results of stability and duration tests performed on these catalysts can be summarized as follows:

- After 30 h CP, loss of alloyed and non-alloyed Co was observed from the Pt–Co/C catalyst, which remains more active than Pt/C. The influence of Co loss on the ORR activity was negligible.
- Thermal treatment at 550 °C increases the particle size for both catalysts, and promotes a Co surface enrichment in Pt–Co/C. The presence of Co metal and its oxides on the catalyst surface hinders molecular oxygen to reach the Pt active sites and the ORR activity was considerably lower than that of Pt.
- Repetitive potential cycling of both as-prepared and thermally treated catalysts gives rise to Pt and Co dissolution and re-deposition of Pt, forming a layer of non-alloyed Pt on the surface of the Pt–Co particles. Thus, the ORR activities of Pt and Pt–Co after RPC were similar, depending only on particle size.

Acknowledgements

SCZ thanks the Conselho Nacional de Desenvolvimento Científico e Tecnológico, CNPq, for a graduate scholarship (Proc. 135911/2006-0). Thanks are also due to FAPESP and CAPES for financial assistance to the project.

References

[1] S. Gottesfeld, T.A. Zawodzinski, in: R.C. Alkire, H. Gerischer, D.M. Kolb, C.W. Tobias (Eds.), Advances in Electrochemical Science and Engineering, vol. 5, 1st ed., Wiley-VCH, Weinheim, 1997, p. 195.
[2] E.I. Santiago, L.C. Varanda, H.M. Villullas, J. Phys. Chem. C 111 (2007) 3146.
[3] S. Koh, J. Leisch, M.F. Toney, P. Strasser, J. Phys. Chem. C 111 (2007) 3744.
[4] S. Koh, C. Yu, P. Mani, R. Srivastava, P. Strasser, J. Power Sources 172 (2007) 50.
[5] P.H. Fernández, S. Rojas, P. Ocón, J.L. Gómez de la Fuente, P. Terreros, M.A. Peña, J.L.G. Fierro, Appl. Catal. B 77 (2007) 19.
[6] J.-S. Do, Y.-T. Chen, M.-H. Lee, J. Power Sources 172 (2007) 623.
[7] S. Koh, M.F. Toney, P. Strasser, Electrochim. Acta 52 (2007) 2765.
[8] Q. Huang, H. Yang, Y. Tang, T. Lu, D.L. Akins, Electrochem. Commun. 8 (2006) 1220.
[9] E. Antolini, J.R.C. Salgado, M.J. Giz, E.R. Gonzalez, Int. J. Hydrogen Energy 30 (2005) 1213.
[10] E. Slavcheva, V. Nikolova, T. Petkova, E. Lefterova, I. Dragieva, T. Vitanov, E. Budevski, Electrochim. Acta 50 (2005) 5444.
[11] J.R.C. Salgado, E. Antolini, E.R. Gonzalez, J. Phys. Chem. B 108 (2004) 17767.
[12] J.R.C. Salgado, E. Antolini, E.R. Gonzalez, J. Electrochem. Soc. 151 (2004) A2143.
[13] J.R.C. Salgado, E. Antolini, E.R. Gonzalez, J. Power Sources 141 (2005) 13.
[14] B.J. Hwang, S.M.S. Kumar, C.-H. Chen, Monalisa, M.-Y. Cheng, D.-G. Liu, J.-F. Lee, J. Phys. Chem. C 111 (2007) 15267.
[15] E. Antolini, J.R.C. Salgado, E.R. Gonzalez, J. Power Sources 160 (2006) 957.
[16] B.C. Beard, P.N. Ross, J. Electrochem. Soc. 137 (1990) 3368.
[17] N. Travitsky, T. Ripenbein, D. Golodnitsky, Y. Rosenberg, L. Burshtein, E. Peled, J. Power Sources 161 (2006) 782.
[18] M. Watanabe, K. Tsurumi, T. Mizukami, T. Nakamura, P. Stonehart, J. Electrochem. Soc. 141 (1994) 2659.
[19] P. Yu, M. Pemberton, P. Plasse, J. Power Sources 144 (2005) 11.
[20] H.R. Colón-Mercado, B.N. Popov, J. Power Sources 155 (2006) 253.
[21] E. Antolini, Mater. Chem. Phys. 78 (2003) 563.
[22] S. Mukerjee, S. Srinivasan, M.P. Soriaga, J. McBreen, J. Electrochem. Soc. 142 (1995) 1409.
[23] V. Jalan, E.J. Taylor, J. Electrochem. Soc. 130 (1983) 2299.
[24] T. Toda, H. Igarashi, H. Uchida, M. Watanabe, J. Electrochem. Soc. 146 (1999) 3750.
[25] V. Stamenkovic, T.J. Schmidt, P.N. Ross, N.M. Markovic, J. Phys. Chem. B 106 (2002) 11970.
[26] V. Stamenkovic, T.J. Schmidt, P.N. Ross, N.M. Markovic, J. Electroanal. Chem. 554/555 (2003) 191.
[27] R.L. Borup, J.R. Davey, F.H. Garzon, D.L. Wood, M.A. Inbody, J. Power Sources 163 (2006) 76.
[28] K.S. Han, Y.S. Moon, O.H. Han, K.J. Hwang, I. Kim, H. Kim, Electrochem. Commun. 9 (2007) 317.
[29] W.E. Triaca, A.J. Arvia, J. Appl. Electrochem. 20 (1990) 347.
[30] L.D. Burke, J.J. Borodzinski, K.J. O'Dwyer, Electrochim. Acta 36 (1990) 967.
[31] L.D. Burke, K.J. O'Dwyer, Electrochim. Acta 37 (1991) 43.
[32] L.D. Burke, M.B.C. Roche, J. Electroanal. Chem. 137 (1982) 175.
[33] K. Kinoshita, J.T. Lundquist, P. Stonehart, J. Electroanal. Chem. Interfacial Electrochem. 48 (1973) 157.
[34] L.D. Burke, E.J.M. O'Sullivan, J. Electroanal. Chem. 112 (1980) 247.
[35] C.C. Hu, K. Liu, Electrochim. Acta 44 (1999) 2727.
[36] K.A. Radyushkina, R.Kh. Burshtein, M.R. Tarasevich, V.V. Kuprina, L.A. Chenyaev, Elektrokhimiya 5 (1969) 1379.
[37] D.A.J. Rand, R. Woods, J. Electroanal. Chem. 36 (1972) 57.
[38] P.N. Ross, K. Kinoshita, A.J. Scarpellino, P. Stonehart, J. Electroanal. Chem. 59 (1975) 177.